HHS Public Access

Author manuscript

Transl Res. Author manuscript; available in PMC 2019 February 01.

Published in final edited form as:

Transl Res. 2018 February ; 192: 1–14. doi:10.1016/j.trsl.2017.10.005.

Induction of innervation by encapsulated adipocytes with engineered vitamin A metabolism

Q. Shen[1,†], **R. Yasmeen**[1,†], **J. Marbourg**[2], **L. Xu**[3,1], **J. L. Yu**[4], **P. Fadda**[5], **A. Flechtner**[6], **L.J. Lee**[7], **P. G. Popovich**[2], and **O. Ziouzenkova**[1,*]

[1]Department of Human Sciences, The Ohio State University, Columbus, Ohio, 43210, USA

[2]Center for Brain and Spinal Cord Repair, The Ohio State University, Columbus, OH 43210, USA; Department of Neuroscience, Wexner Medical Center, The Ohio State University, Columbus, OH 43210, USA

[3]Department of Minimally Invasive Surgery, The First Affiliated Hospital of Soochow University, Suzhou, Jiangsu, China

[4]Department of Statistics, The Ohio State University College of Medicine, Columbus, OH 43210, USA

[5]Nucleic Acid Shared Resource, Comprehensive Cancer Center, The Ohio State University, Columbus, Ohio 43210, USA

[6]Histology and Immunohistochemistry Laboratory, The Ohio State University, Columbus, Ohio, 43210, USA

[7]Department of Chemical and Biomolecular Engineering, The Ohio State University, Columbus, Ohio, 43210, USA

Abstract

Innervation is a fundamental basis for function and survival of tissues. In the peripheral tissues, degenerative diseases create a neurotoxic metabolic milieu that either causes neurodegeneration or fails to sustain regenerative growth and re-innervation of injured/diseased tissues. Encapsulation of cells producing neurotrophic factors can augment axon growth and neuron survival; however, sustained innervation in vivo requires a combination of factors promoting axon growth and guidance pathway that are released in a tissue-specific context. Using novel encapsulation techniques and genetic tools, we manipulated retinoic acid-generating enzyme aldehyde dehydrogenase 1a1 (*Aldh1a1)* in adipocytes that is capable of promoting growth and innervation

*To whom correspondence should be addressed: Ouliana Ziouzenkova, PhD, 1787 Neil Avenue, 331A Campbell Hall; Columbus, OH 43210, ziouzenkova.1@osu.edu; Telephone: 001 614 292 5034; Fax: 001 614 292 8880.
†Both authors contributed equally to this work

The authors declare that they have no conflict of interests.

CONFLICT OF INTERESTS

The authors declare that they have no conflicts of interests.

of white adipose tissue (WAT) by sympathetic neurons. *Aldh1a1*$^{-/-}$ adipocytes secrete molecules that regulate axon-guidance and markedly stimulate neurite outgrowth in vitro and in vivo. Based on studies with natural and synthetic RAR agonists and antagonists, gene microarray and nanostring arrays, we concluded that ephrin A5/ephrin A4 is a downstream pathway regulated by *Aldh1a1*. Encapsulation of *Aldh1a1*$^{-/-}$ adipocytes into alginate poly-L-lysine microcapsules induced functional innervation of adipose tissue in obese wild-type mice. We propose that encapsulated *Aldh1a1*$^{-/-}$ adipocytes could provide a therapeutic solution for the reinnervation of damaged tissues.

INTRODUCTION

Neuronal damage [1, 2] and neurodegeneration [3–5] impair central nervous system (CNS) function, they play critical role in the development and progression of metabolic disorders [6, 7]. Axons provide a template for vascularization [8]. Additionally, axons integrate responses between peripheral tissues and the CNS [9]. Sympathetic innervation of white adipose tissue (WAT) controls essential metabolic processes such as lipolysis and energy dissipation by thermogenic adipocyte [10, 11]. Malfunctions in lipolysis and thermogenesis are associated with obesity [12]. Although the critical role for peripheral innervation in tissue homeostasis is well established, researchers still face considerable challenges in rebuilding axonal circuits after metabolic damage or injuries.

A significant challenge for rebuilding neuronal circuits is the failure of CNS axons to regenerate after injury. Peripheral nervous system (PNS) axons are capable of regeneration [13] and, thus, represent a more viable target for regeneration therapies. Such therapies typically focus on improving neuron survival and enhancing axon growth [14]. Even though PNS nerves can regenerate [15], functional regeneration is often incomplete, due to decreased trophic support from peripheral cells [16]. One way to enhance the growth-supportive milieu for axons is to provide engineered encapsulating cells into preferred target sites. Cell encapsulation appears to be a safe and sustainable approach to deliver desirable compounds, such as NGF or brain-derived neurotrophic factor (BDNF), to the brain and other tissues [17, 18]. Although treatment with neurotrophic factors improves neuronal survival, it lacks other cues that guide axons and enable the formation of functional networks. These cues include axon guidance molecules (for attraction and repulsion), specific proteases, and other regulatory molecules responsible for regulation of G-proteins signaling cascades [8]. Together these cues allow for the formation of specific neuronal networks between peripheral tissues and the CNS. Because it is not conceivable to engineer cells to express all these molecules, it is critical to identify cells and/or regulatory pathways upstream of the production of axon guidance cues.

One such cell type is preadipocytes/fibroblasts. Preadipocytes have been identified as a common environment of peripheral vascular innervation [19]. Preadipocytes also play an important role in intracrine and paracrine regulation. Specifically, preadipocytes produce metabolites of vitamin A, such as retinoic acid (RA) and retinaldehyde (Rald) (Figure 1A) [20]. RA acts as an ligand for the retinoic acid receptor (RAR) and activates transcriptional or translational responses of RAR [21]. This receptor plays an important role in both

thermogenesis and differentiation of neurons [21–23]. In preadipocytes and adipocytes, intracellular production of RA regulates adipogenesis and adipokine production [21]. Additionally, RA could potentially regulate de novo neurogenesis from stromal cells in a paracrine fashion [22]. RAR activation in adipocytes depends on the aldehyde dehydrogenase 1 (ALDH1A1) enzyme [20]. Surprisingly, *Aldh1a1*$^{-/-}$-deficient mice producing 70% less RA [22] also exhibit increased thermogenesis in WAT [24, 25]. Whether increased thermogenesis in *Aldh1a1*$^{-/-}$ mice is associated with improved sympathetic innervation it unknown [11]. Here, we identified a role for *Aldh1a1*$^{-/-}$ preadipocytes in the production of axon guidance molecules in vivo and in vitro and established a connection between increased WAT innervation and metabolic rate in mice engrafted with *Aldh1a1*$^{-/-}$ adipocytes.

EXPERIMENTAL AND METHODS

Animal studies

Animal studies were approved by the Institutional Animal Care and Use Committee of The Ohio State University (OSU). Data for all studies are summarized in Table S1. The exclusion criteria was the loss of more than 20% of weight in the course of the study; however, no animal was excluded from this study.

Randomization strategy. In studies 1 and 2 mice were randomized into age matching groups with similar percent of male and female mice. For proof-of concept study 3 we used only aged-matched female mice to match sex of implanted immortalized fibroblasts. Mice were randomly selected into control and treatment groups.

1.1. Study 1. WT and *Aldh1a1*$^{-/-}$ mice on a high-fat (HF) diet—

Aldh1a1$^{-/-}$ deficient mice (C57BL/6J background) were developed and provided by G. Duester and colleagues [26] and their metabolic profile was described [20, 24, 27–29]. Matched C57BL/6 (WT) mice were used as control. C57BL/6J (WT) mice were initially purchased from The Jackson Laboratory (Bar Harbor, ME) and then bred at OSU. Mice were fed a regular chow diet (Harlan Teklad, Madison, WI). We used power analysis to determine the sample size of this study based on data from study [30]; however, more animals were enrolled to complete all analysis.

WT and *Aldh1a1*$^{-/-}$ were fed a high fat diet (HF, 45% kcal from fat, D12451, Research Diet Inc., New Brunswick, NJ) for 180 days (8 month old at dissection) (Numbers, sex, weight are described in Supplementary Table S1). Visceral (intra-abdominal (i-Ab); gonadal) fat was collected for protein, mRNA, and histology. To omit a concern of heterogeneity of adipose tissue, regarding thermogenic/lipogenic adipocyte composition and innervation, we used the whole fat pad for each analysis. For example, we used the whole left fat pad for mRNA analysis and the right for the protein analysis. For histochemistry and NE extraction we used another group of randomly selected animals from the same large study. The number of animals that were randomly selected for specific analysis were smaller than the number of animals in the whole group and are described in figure legends.

Study 2. Comparison of WT and *Aldh1a1*$^{-/-}$ mice on a regular chow diet—Five-month old WT and *Aldh1a1*$^{-/-}$ mice (numbers, sex, weight are described in Supplementary Table S1) were fed a regular chow diet (Harlan Teklad, Madison, WI). WAT and EDTA-plasma was collected for analysis and stored at −80°C.

Study 3. WT mice on a high-fat (HF) diet treated with encapsulated WT adipocytes and *Aldh1a1*$^{-/-}$ adipocytes—The immortalized WT and *Aldh1a1*$^{-/-}$ were derived from females [28], therefore, we used females for this mechanistic proof-of-concept study. Encapsulation into alginate-poly-L-lysine is described in a detailed video protocol [31]. Eighteen 4-month old WT female mice (C56BL/6J, The Jackson Laboratory, Bar Harbor, ME, breed at OSU) were fed a HF diet for 220 days to induce obesity (N=18; Supplementary Table S1). After that period, mice were randomly assigned into four groups: 1) injected with vehicle (1mL sterile PBS, n=5); 2) acellular 'empty' capsules (n=3); 3) encapsulated WT fibroblasts (0.5×10^6 cells in 1 mL PBS per iAb depot, n=5); and 4) encapsulated *Aldh1a1*$^{-/-}$ preadipocytes (0.5×10^6 cells in 1 mL PBS per iAb depot, n=5). Mice were injected with vehicle or encapsulated cells into both iAb depots, and maintained on the same HF diet for additional 80 days. The induction of thermogenesis by encapsulated *Aldh1a1*$^{-/-}$ under these conditions is described in [28]. Whole iAb fat, which contains all encapsulated and host cells, was collected for protein analysis. Another iAb fat pad was embedded into paraffin for histological examination of innervation.

Metabolic measurements—Metabolic parameters were measured by indirect calorimetry (CLAMS, Columbus Instruments, Columbus, OH) at ambient temperature (22°C) with 12h light/dark cycles. Animals were fed the same HF diet and water was provided *ad libitum*. Mice were housed individually and allowed to acclimatize in the chambers for 12h. Oxygen consumption, CO_2 production, energy expenditure, and locomotor activity were measured for at least 24h. Based on these data, respiratory quotient or exchange ratio (V_{CO2}/V_{O2}) and heat values were calculated by CLAMS.

Norepinephrine (NE) measurements—Norepinephrine was measured in plasma and fat samples using Noradrenaline High Sensitive ELISA (EA633.96, Eagle Biosciences/DLD Diagnostika Hamburg, Germany) according to manufacturer's instructions. Hemolysed blood samples were excluded as recommended by manufacturer. For analysis the whole fat pad (inguinal, i-Ab, or two brown fat pads) was homogenized using phosphate buffered saline.

Cell culture studies

Stromal vascular fraction (SVF) and immortalized cell line development—SVF was isolated from subcutaneous fat of one-month-old WT and *Aldh1a1*$^{-/-}$ female mice fed regular chow as described [30]. Fibroblasts (preadipocytes) from SVF were immortalized using the protocol described in [28]. The phenotype of these cells was validated using Affimetrix gene microarray (described below). Full gene expression data set is uploaded as GEO file: 'QS wild type and Aldh1a1 KO preadipocytes 2015'.

Preparation and stimulation of adult mouse dorsal root ganglion (DRG) neurons—Single cell suspensions from cervical, thoracic, and lumbar DRG neurons were isolated from terminally anesthetized C57BL/6 adult female mice (12–16 weeks old, regular chow, The Jackson Laboratory) [32]. Overall three mice were purchased for DRG isolation and these mice were not a part of other studies. Dissected DRGs were enzymatically digested in a solution of collagenase type 2 (200 U/mL; Sigma-Aldrich C6885, St. Louis, MO) and dispase I (5U/mL; Sigma-Aldrich D4818) on a shaker for 45 min at 37°C [32]. Enzyme solution was aspirated and cells were washed twice in Hank's Balanced Salt Solution 1× (HBSS; Mediatech Inc., Manassas, VA) before incubating in DNase I type II (5mg/mL; Worthington Biochemical, Lakewood, NJ) for 5 min at room temperature. DRGs were triturated in HBSS with Pasteur pipette until cells were well dissociated, then passed through a Falcon 70μm cell strainer (Corning Inc., Corning, NY) to remove myelin debris, After a 3 min centrifugation at 3,000 rpm to pellet the cells. The neuron-enriched pellet was resuspended in DRG culture medium (DMEM/F12, 1% N2 supplement, and 0.05% Gentamicin) and live cells were counted on a hemocytometer using trypan blue exclusion. Cells were plated at 500 cells/well in a 24-well plate (Corning Inc.) previously coated with poly-D-lysine (25ug/mL; Sigma-Aldrich P6407) and laminin (10 μg/mL; Thermo Fisher Scientific 23017015, Grand Island, NY). Each batch of DRG neurons were incubated at 37°C/5% CO_2 in DRG culture medium only, DRG culture medium with NT-3 (1 ng/mL), with NGF (10 ng/mL), with WT secretome, with DRG medium (1:1, v/v), and with *Aldh1a1*$^{-/-}$ secretome with DRG medium (1:1, v/v) for 24 hours. To assess neurite outgrowth and neuronal morphology, cells were fixed with 4% paraformaldehyde for 25 min [33] and washed in 0.1 M PBS, then incubated in blocking solution (4%BSA/0.3% Tx-100/PBS) for 1 hr at room temperature. Cells were immunostained with a monoclonal neuronal anti-β-tubulin III antibody (Sigma-Aldrich, T8578). Antibody was diluted in blocking solution (1:1000; at 4°C overnight), then washed and incubated in Alexa Fluor 546 secondary antibody (1:1000; Thermo Fisher Scientific Z25004) for 1 h at RT. Cells were automatically imaged using a Thermo Scientific™ ArrayScan™ XTI Live High Content microscope and analyzed with the Neuronal Profiling algorithm in the HCS Studio™ software (Thermo Fisher Scientific) [34]. Total neurite length, average neurite length, number of branch points, critical value, dendrite maximum, and ramification index were averaged across all neurons detected per well, with 3 wells included per treatment. Three experimental replicates were performed using DRGs from three mice (total: n=9). Dendrite maximum and critical value are parameters determined based on Scholl analysis. These values were automatically generated by the software. Dendrite maximum corresponds to the maximum number of dendrite crossings at a given radius from the cell body, and the critical value describes the radius at which the dendrite max occurs. The ramification index of a neuron is the dendrite max value divided by the number of primary dendrites. Percent of neurons with neurites was calculated as the ratio of the number of neurons with neurite extension to the total number of neurons per well. Significant growth differences were calculated in GraphPad Prism 5.0 (GraphPad Software) using well averages in a one-way ANOVA followed by a Tukey *post-hoc* analysis. Differences were significant for p<0.05.

Adipocyte differentiation—Murine preadipocyte (3T3-L1, WT, and *Aldh1a1*$^{-/-}$) lines were cultured and maintained in standard culture medium (DMEM containing 10% calf

serum and 0.1% 50 mg/mL gentamicin). Adipogenesis was induced (Day 0) in confluent preadipocytes using differentiation medium I containing 3-isobutyl-1-methylxanthine (0.5mM), dexamethasone (1μM), insulin (1.7μM), 10% FBS, and 0.1% gentamicin in DMEM. Differentiation medium II containing 10% FBS, insulin (1.7μM), and 0.1% gentamicin in DMEM was replaced every 48 h after adding differentiation medium I.

Gene expression analysis

Affymetrix GeneChip—mRNA was isolated by RNeasy (Qiagen, Valencia, CA). RNA integrity was interrogated using an Agilent 2100 Bioanalyzer (Agilent Technologies). A 100 ng aliquot of total RNA was linearly amplified. Then, 5.5μg of cDNA was labeled and fragmented using the GeneChip WT PLUS reagent kit (Affymetrix, Santa Clara, CA) following the manufacturer's instructions. Labeled cDNA targets were hybridized to Affymetrix GeneChip Mouse Gene ST 2.0 arrays for 16 h at 45 °C rotating at 60 rpm. The arrays were washed and stained using a Fluidics Station 450 and scanned using a GeneChip Scanner 3000. Signal intensities were quantified by Affymetrix Expression Console version 1.3.1. Background correction and quantile normalization were performed to adjust for technical bias, and probe-set expression levels were calculated by the RMA method. After filtering above noise cutoff, there are 9,528 probe-sets that were tested by linear model. A variance smoothing method with fully moderated t-statistic was employed for this study and was adjusted by controlling the mean number of false positives. With a combined cutoff of 2-fold change and p-value of 0.0001 (controlling 1 false positive over all probe-sets), we declared 500 probe-sets as differential gene expression between *Aldh1a1*$^{-/-}$ and WT preadipocytes. GEO file: 'QS wild type and Aldh1a1 KO preadipocytes 2015'.

NanoString nCounter gene expression assay—NanoString's nCounter analysis (NanoString Technologies) system performed direct detection of target molecules from a single sample using color-coded molecular barcodes, giving a digital quantification of the number of target molecules as described before [35]). A custom panel containing axon guidance molecules was designed and used for simultaneous quantification of 32 axon guidance genes and 5 housekeeping genes. All data were normalized to 5 housekeeping genes quantified in the same samples. Total mRNA (100ng in 5ul) was hybridized overnight with nCounter Reporter (20μl) probes in hybridization buffer and in an excess of nCounter Capture probes (5μL) at 65°C for 16–20h. The hybridization mixture containing target/probe complexes was allowed to bind to magnetic beads containing complementary sequences on the Capture Probe. After each target found a probe pair, excess probes were washed followed by sequential binding to sequences on the Reporter Probe. Biotinylated capture probe-bound samples were immobilized and recovered on a streptavidin-coated cartridge. The abundance of specific target molecules was then quantified using the nCounter Digital Analyzer. Individual fluorescent barcodes and target molecules present in each sample were recorded with a CCD camera by performing a high-density scan (600 fields of view). Images were processed internally into a digital format and were normalized using the NanoString nSolver software analysis tool. Counts were normalized for all target RNAs in all samples based on the positive control RNA to account for differences in hybridization efficiency and post-hybridization processing, including purification and immobilization of complexes. The average was normalized by background counts for each sample obtained from the average of

the eight negative control counts. Six internal reference housekeeping genes: Gapdh, Gusb, Hprt1, Pgk1, and Tubb were analyzed. Subsequently, a normalization of mRNA content was performed based on these genes, using nSolver Software

Semi-quantitative mRNA analysis—mRNA was isolated from WAT or adipocyte cultures according to the manufacturer's instructions (Qiagen; Valencia, CA). cDNA was prepared from purified mRNA and analyzed using a 7900HT Fast Real-Time PCR System, TaqMan fluorogenic detection system, and validated primers (Applied Biosystems; Foster City, CA). Comparative real time PCR was performed in triplicate, including no-template controls. mRNA expression of genes of interest was normalized by Tata box protein (TBP) or18S expression level using the comparative cycle threshold (Ct) method.

Protein analysis

Immunohistochemistry—Fat pads were embedded into paraffin for immunohistochemical analysis. Sections were stained with hematoxylin and eosin (H&E) using a modified hematoxylin procedure followed by dehydration in graded alcohol or with peripherin (Abcam, ab4666, Cambridge, MA) and tyrosine hydroxylase polyclonal rabbit antibodies (Abcam, ab41528, Cambridge, MA) at 1:1000 dilution. Images were obtained using Olympus M081 IX50 and Pixera Viewfinder 3.0 software.

Western blot—Cell/tissue protein lysates were normalized by protein content (BCA, Thermo Fisher Scientific). Medium was collected from cells, which were plated at similar numbers. Protein lysate or medium were separated on 10% acrylamide gel under reducing conditions. After transfer to a polyvinylidene fluoride membrane (Immobilon-P; Millipore), proteins were analyzed using an Odyssey Infrared Imaging System (LI-COR Biosciences). EFNA5 (Abcam, ab70114, Cambridge, MA), peripherin, and tyrosine hydroxylase polyclonal rabbit antibodies (same as in immunohistochemistry) were used at 1:1000 dilution.

Enzyme-linked immunosorbent assay (ELISA)—Plasma samples were collected from WT and *Aldh1a1*$^{-/-}$ (A1KO) mice in Study 1–3. Adipose tissues were homogenized in radio immunoprecipitation assay (RIPA) buffer and used at same protein concentration (50μg/mL). Medium was collected from differentiated and non-differentiated 3T3-L1. Absorbance (450 nm) was measured using a Synergy H1 Hybrid Multi-Mode Microplate Reader. NGF ELISA was purchased from Abnova (KA0400, Walnut, CA) and used to measure media from WT and *Aldh1a1*$^{-/-}$ adipocytes and plasma from WT and *Aldh1a1*$^{-/-}$ mice.

Statistical analysis

Blinding statement: The mice treatment and collection of metabolic data and analysis of mRNA samples and immunohistochemistry was performed by different groups on coded samples. Human samples were obtained at Mayo clinic, and animal studies were performed by Ms. Shen and Yasmeen, who were responsible for the sample coding. The coded animals were placed in metabolic cages facility supervised by the Department of Physiology and data were collected and digitalized. mRNA and gene array was performed on coded samples

at Nucleic acid facility and Dr. Fadda performed basic normalization on coded samples. Statistical analysis was performed by Dr Yu at the statistical department, who was provided with the decoding information. Dr. Flechtner performed immunohistochemistry on coded samples. Ms. Marbourg performed DRG experiments and axon outgrowth for each condition without knowledge to treatment. Unbiased analyses of axon growth were conducted using software (HCS Studio™ software) associated with an automated high-content image analysis system.

All data are reported either as mean±standard deviation (s,d.) or mean± standard error (s.e.m). Number of samples is indicated in figure legends and Supplementary Table S1. Normal distribution was tested using Shapiro-Wilk test. Group comparisons were assessed using Mann Whitney U test, and/or ANOVA models or Kolmogorov-Smirnov test. All tests were two-sided. $P<0.05$ was considered to be statistically significant and is presented as asterisk (*). Trends were examined using Pearson correlation analysis tests.

Supporting Information Available

Supplementary Table S1, and Supplementary Figure S1 are provided.

RESULTS

Aldh1a1 in WAT creates a permissive environment for neural innervation

We investigated the cumulative impact of *Aldh1a1* deficiency in peripheral innervation in mice adipose tissue. NGF was the first neurotrophic factor, which was described in adipocytes to be associated with obesity and vitamin A [36–38]. NGF levels in the circulation were similar in WT and *Aldh1a1*$^{-/-}$ mice fed a regular (Figure 1B, Study 2) and a high fat chow (HF, Figure 1C, Study 1). Next, we compared expression of neuronal markers in WT and *Aldh1a1*$^{-/-}$ male and female mice developing different WAT mass on a HF diet. Expression of *Rbfox3* (Figure 1D), a marker of the mature neurons, was similar in WAT of WT and *Aldh1a1*$^{-/-}$ male and female mice on a HF diet. The expression of the neuronal precursor markers *nestin* (Figure 1E) and *synapsin* (Figure 1F) was significantly reduced in *Aldh1a1*$^{-/-}$ compared to WT mice on a HF diet. These data suggest diminished *de novo* neurogenesis from the stromal cells or preadipocytes. This was expected due to diminished RA production in WAT in *Aldh1a1*$^{-/-}$ *vs.* WT adipocytes [20] and in the circulation [39]. Sprouting and growth of axons could increase innervation [11]. We observed higher protein expression in peripherin and tyrosine hydroxylase (TH), markers of peripheral and sympathetic neurons, respectively in *Aldh1a1*$^{-/-}$ *vs.* WT WAT (Figure 1G, H). The increased innervation was associated with significantly higher levels of norepinephrine (NE) in WAT of *Aldh1a1*$^{-/-}$ compared to WT mice (Figure 1I). We hypothesized that *Aldh1a1*$^{-/-}$ preadipocytes and/or adipocytes release signals promoting innervation by growing axons.

Aldh1a1$^{-/-}$ adipocytes stimulate growth in dorsal root ganglion (DRG) neurons in vitro

To prove that molecules secreted from *Aldh1a1*$^{-/-}$ preadipocytes can directly influence neurons, we stimulated neurons with a medium from differentiated WT and *Aldh1a1*$^{-/-}$ adipocytes. For all experiments, we isolated an equal number of DRG neurons, 500 per well.

Axonal growth in media from *Aldh1a1*$^{-/-}$ adipocytes was significantly more extensive than that seen in the presence of the classic inducers, NGF (Figure 2A, B, larger numbers are shown in Supplementary Figure S1). Stimulation of primary murine DRG neurons with the medium obtained from differentiated *Aldh1a1*$^{-/-}$ adipocytes led to a marked induction of axonal growth. We quantified axon growth by total length (Figure 2C), average length (Figure 2D), total branching points (Figure 2E), dendrite max (Figure 2F), as well as ramification index (Figure 2G) and critical values calculated from these parameters (Figure 2H). All parameters showed that media from differentiated *Aldh1a1*$^{-/-}$ adipocytes *vs*. WT adipocytes markedly increased axon growth. Endogenous levels of NGF were present in low and equal amounts in the media from WT adipocytes and *Aldh1a1*$^{-/-}$ adipocytes (0.1ng/mL compared to 10ng/mL of NGF used for positive control) (Figure 2I). Thus, molecules secreted from *Aldh1a1*$^{-/-}$ adipocytes are neurotrophic and promote robust axon growth.

RA suppressed the positive regulation of axon growth by *Aldh1a1*$^{-/-}$ secretome

To test the role of RA in regulation of axon-guiding mediators in *Aldh1a1*$^{-/-}$ adipocytes, we differentiated *Aldh1a1*$^{-/-}$ preadipocytes in the presence or absence of RA. Then we cultured naïve primary DRG neurons in this medium. The RA-conditioned *Aldh1a1*$^{-/-}$ secretome inhibited the growth of DRG axons relative to the neurotrophic media from *Aldh1a1*$^{-/-}$ adipocytes (Figure 3A, B). Thus, intracrine regulation of RA production from Rald by ALDH1A1 may be a mechanism by which adipocytes control innervation.

Aldh1a1 regulates genes involved in axon guidance

We compared genome of WT and *Aldh1a1*$^{-/-}$ preadipocytes using gene microarray (Figure 4A). Pathway analysis revealed that the primary pathway altered in *Aldh1a1*$^{-/-}$ vs. WT adipocytes was the axon guidance (Figure 4A). Axon guidance pathway includes axon guidance molecules *Efna5, Sema3d*, *Sema3e*, their receptors and co-regulatory molecules *Epha4, Slit1, Robo1, Hhip*. [40, 41] Axon growth is dependent on proteolysis that enables remodeling of matrix proteins and cleavage-dependent activation and secretion of ephrin ligands [42, 43]. Within the *Aldh1a1*$^{-/-}$ -axon guidance pathway, there was significantly increased expression of mRNA encoding the proteases *AdamtS9*, matrix metallopeptidase 10 (*Mmp10*), and *Mmp13* in *Aldh1a1*$^{-/-}$ compared to WT adipocytes. The changes in expression of all these genes were validated using the quantitative nanostring approach (Figure 4B–E).

To elucidate if *Aldh1a1* could be involved in the cumulative regulation of genes responsible for axon guidance, we stimulated *3T3-L1* adipocytes with natural vitamin A metabolites controlled by this enzyme: 1) RA and 2) Rald, a RA precursor present in *Aldh1a1*$^{-/-}$ adipocytes [27]. We also compared these responses to synthetic RAR agonist TTNPB and antagonist BMS493. We have found that Rald significantly induced the expression of *Sema3e*, *AdamtS9*, and *Efna5* in *3T3-L1* adipocytes (Figure 4F). However, the ability of Rald to induce expression of *Sema3e* and *AdamtS9* occurs independently of RAR agonists or antagonists (Figure 4G). In contrast, expression of *Epha4* and *Efna5* was increased in the presence of the RAR inhibitor, BMS493, and suppressed by the RAR ligand, TTNPB (Figure 4H), suggesting direct regulation by RAR. In a loss-of-function experiment, the addition of an anti-EFNA5 antibody prevented outgrowing of neurites and decreased their

maximum length following stimulation by *Aldh1a1*$^{-/-}$ media (Figure 4I). Other parameters, such as total branch point, were not influenced by this treatment. These data suggest that complete *Aldh1a1*$^{-/-}$ secretome is required to achieve full axonal growth efficiency, although EFNA5 contributes to the axon growth-promoting activity of *Aldh1a1*$^{-/-}$ adipocytes.

Encapsulated *Aldh1a1*$^{-/-}$ adipocytes induce innervation in WAT of WT obese mice

To study if *Aldh1a1*$^{-/-}$ adipocytes could be used to stimulate innervation in vivo, we used a previously established model for testing encapsulated cells for metabolic disease treatment [28, 31]. Semipermeable poly-L-lysine membrane allows encapsulated cells to exchange low molecular weight molecules (<36kD) [28]. Here we used same model to study paracrine effects of axon guidance molecules, because *Efna5* gene encodes 26kD protein.

We prepared equal concentrations of empty acellular capsules, encapsulated WT, as well as *Aldh1a1*$^{-/-}$ adipocytes as previously described [31]. Host obese WT mice were treated using encapsulated WT adipocytes (Control), *Aldh1a1*$^{-/-}$ adipocytes, or acellular capsules (acellular control). Capsulates were injected into WAT of obese WT host mice Study 3. After 80 days post-treatment WAT were isolated and used for analysis of innervation. Encapsulated *Aldh1a1*$^{-/-}$ adipocytes, but not WT adipocytes, stimulated the development of peripherin-positive axons around the capsules (Figure 5A). Peripherin expression in WAT injected with encapsulated *Aldh1a1*$^{-/-}$ adipocytes was significantly higher than in WAT injected with empty capsules (Figure 5B). Tyrosine hydroxylase (TH)-positive sympathetic axons were also present around *Aldh1a1*$^{-/-}$ capsules, but neither proximal or distal to encapsulated WT adipocytes (Figure 5C). No detectable nerves were found in adipose tissue in non-treated obese mice or mice treated with acellular capsules. Mice treated with encapsulated *Aldh1a1*$^{-/-}$ adipocytes had increased metabolic rate during the active (dark) period (Figure 6A). This change was not due to differences in food consumption (Figure 6B), as mice injected with encapsulated WT and *Aldh1a1*$^{-/-}$ cells had similar food intake. The development of sympathetic innervation (Figure 6C) was associated with the formation of thermogenic UCP-1 positive adipocytes clusters in obese WT mice treated with encapsulated *Aldh1a1*$^{-/-}$ adipocytes described previously [28]. No such effect was seen in control groups. Thus, paracrine effects from a subset of encapsulated *Aldh1a1*$^{-/-}$ adipocytes promote functional innervation of WAT in vivo.

DISCUSSION

Our studies revealed a specific paracrine role of *Aldh1a1*$^{-/-}$ adipocytes in the regulation of axon-guidance pathway molecules that support the induction of sympathetic innervation. Moreover, encapsulation of *Aldh1a1*$^{-/-}$ adipocytes in alginate poly-L-lysine capsules is a viable strategy for boosting sympathetic innervation of WAT over a long period. Indeed, conditioned medium from *Aldh1a1*$^{-/-}$ adipocytes has potent growth-promoting effects and encapsulation of these adipocytes with subsequent transplantation into WAT maintains their growth-promoting potential *in vivo*. Encapsulation technology has been previously developed for the implantation of pancreatic beta islet for insulin production [44, 45]. Here we show that a subset of encapsulated cells with the engineered paracrine mechanism can

alter expression of multiple genes and orchestrate a complex innervation process. This technology holds the potential to stimulate axonal growth in translational settings for the treatment of metabolic neuropathies and, potentially, injuries and degenerative disease of the CNS.

Studies in animal models of obesity, as well as epidemiologic and clinical evidence, suggest a pathophysiologic relationship between neuropathy and metabolic syndrome [46]. Lipolysis and thermogenesis induction depend on a sensory-sympathetic circuit [10, 11]. Researchers have shown that lipid-storing adipocytes in WAT contribute to the production of axon guiding molecules associated with obesity [38, 47]. Accordingly, the levels of these molecules, such as NGF [37, 38] and SEMA3A [47] are increased in obese patients. We provide evidence of another pathway in which *Aldh1a1*$^{-/-}$ adipocytes produce distinct guidance cues for sensory axons and establish the inflow from WAT to the brain for the induction of sensory-sympathetic circuit and thermogenesis (Figures 5 and 6).

The key role of ALDH1A1 is in the production of RA from the precursor Rald with downstream activation of RAR in adipocytes [20]. We have shown that Rald can induce expression of *Efna5/Epha4* genes. Conversely, conversion of Rald to RA activated RAR and reduced EFNA5 expression and secretion, Therefore, *Efna5/Epha4* appear to be the primary target of vitamin A pathway that is responsible for innervation. It is possible that activated RAR also regulate other genes, such as Sema3e. Even though multiple genes are involved in axonal guidance, RAR exerts the overall control over peripheral innervation. Inhibition of RAR decreased neurogenesis, instead, increased EFNA5 expression and secretion stimulated sensory-sympathetic innervation and adaptive thermogenesis. These responses place ALDH1A1 in a central regulatory position switching between lipogenic and thermogenic innervation in WAT.

Several questions remain unanswered from our study. What types of cells are suitable for encapsulation technology and for guidance of specific neurons subtypes? Many empirical studies have indicated that stem cells in adipose tissue can improve recovery from spinal cord injuries [48]. Other researchers have noted that implants of thermogenic beige and brown adipocyte become innervated, without explaining the mechanism of this phenomenon [49]. It is unclear if these cells play a paracrine role in innervations or differentiate precursor cells into neurons. Importantly, small populations of adipocytes in WAT can produce cues to promote *de novo* innervation and can be used for encapsulation technology. More research is needed to clarify the composition of molecules associated with axon guidance, which could include microRNA and/or metabolites. We did not investigate these molecules in current study. Recent studies showed that *AdamtS9* is a gene associated with sexual dimorphism in fat distribution [50] as well as susceptibility to type 2 diabetes in adults [51] and children [52]. Further studies are needed to elucidate if *AdamtS9* supports the EFNA5/EPHA4 pathway of axon growth and if it contributes to the role of EFNA5 in obesity. The primary goal of this study was to prove that *Aldh1a1*$^{-/-}$ adipocytes use a paracrine mechanism to induce axon growth in WAT. In vitro, the secretome of *Aldh1a1*$^{-/-}$ adipocytes robustly induced neurite outgrowth in DRG neurons and its activity exceeded effects of the classic inducers, NGF and NT-3. In vivo, only encapsulated *Aldh1a1*$^{-/-}$ adipocytes, stimulated innervation in WAT of obese WT host mice. The nerves adjacent to encapsulated *Aldh1a1*$^{-/-}$

adipocytes were peripherin- and TH-positive, indicating sympathetic innervation. This innervation was associated with increased NE secretion and converted adipocytes of obese WT animals into thermogenic UCP1-positive multilocular adipocytes. This conversion increased the metabolic rate of treated animals. The remodeling of host WAT occurred distally from capsules by means of the outgrowth of host TH-positive sympathetic neurons. Therefore, paracrine mediators from *Aldh1a1*$^{-/-}$ adipocytes, acting via the sympathetic nerves system, have a higher capacity for thermogenic remodeling than stimulation of an intracellular thermogenic machinery in beige or brown adipocytes. This autonomous mechanism induced by encapsulated engineered cells offers an opportunity for treatment of obesity in a fat depot-specific manner.

Supplementary Material

Refer to Web version on PubMed Central for supplementary material.

Acknowledgments

We would like to thank Alessandro Brunetti, Jennifer Wall, and Jack Leung (The Ohio State University) for their editorial help. This research was supported by the Ray W. Poppleton Endowment (P.G.P.), and NSF Center funding (EEC-0914790). The project was supported by NIH grants R21OD017244 (O.Z.), R01NS047175 (P.G.P.), R00 HL121284-01 (F.A), the National Center for Research Resources UL1RR025755, UL1TR001070, and NCI P30CA16058 (OSUCCC), and the NIH Roadmap for Medical Research. The content is solely the responsibility of the authors and does not necessarily represent the official views of the National Center for Research Resources or the National Institutes of Health. This research was supported by the SEED Grant from College of Education and Human Ecology, Accelerator Grant from Office for International Affairs, and Center for Advanced Functional Foods Research and Entrepreneurship at OSU (O.Z.). The content is solely the responsibility of the authors and does not necessarily represent the official views of the National Center for Advancing Translational Sciences. All authors have read the journal's authorship agreement and the manuscript has been reviewed by and approved by all named authors.

Abbreviations

A1KO	Aldehyde dehydrogenase 1 A1 deficient mice (*Aldh1a1*$^{-/-}$)
Aldh1a1	Aldehyde dehydrogenase family 1 member A1
ANOVA	Analysis of variance
CNS	Central nervous system
DRG	Dorsal root ganglia
EFNA5	Ephrin A5 ligand
ELISA	Enzyme-linked immunosorbent assay
EPHA4	Ephrin A4 receptor
iAb	intra-abdominal or visceral fat
HF	High-fat
Mmp	Matrix metallopeptidase
NE	Norepinephrine

NGF	Nerve growth factor
PBS	Phosphate buffered solution
PNS	Peripheral nervous system
RA	Retinoic acid
Rald	Retinaldehyde or retinal
RAR	Retinoic acid receptor
rEFNA5	Recombinant ephrin A5
RER	Respiratory exchange ratio
ROL	Retinol
RT	Room temperature
Sema3e	Semaphorin 3e
Sema3d	Semaphorin 3d
SNS	Sympathetic nervous system
TBP	Tata box protein
TH	Tyrosine hydroxylase
TTNPB	Arotinoid acid or 4-[(E)-2-(5,6,7,8-Tetrahydro-5,5,8,8-tetramethyl-2-naphthalenyl)-1-propenyl]benzoic acid (high affinity RAR agonist)
UCP1	Uncoupling protein 1
Veh	Vehicle
WAT	White adipose tissue
WT	Wild type

References

1. Inskip J, Plunet W, Ramer L, et al. Cardiometabolic risk factors in experimental spinal cord injury. Journal of neurotrauma. 2010; 27(1):275–85. DOI: 10.1089/neu.2009.1064 [PubMed: 19772460]
2. Edwards LA, Bugaresti JM, Buchholz AC. Visceral adipose tissue and the ratio of visceral to subcutaneous adipose tissue are greater in adults with than in those without spinal cord injury, despite matching waist circumferences. Am J Clin Nutr. 2008; 87(3):600–7. doi. [PubMed: 18326597]
3. Hetz C, Saxena S. ER stress and the unfolded protein response in neurodegeneration. Nature reviews Neurology. 2017; doi: 10.1038/nrneurol.2017.99
4. Rojas-Gutierrez E, Munoz-Arenas G, Trevino S, et al. Alzheimer's disease and metabolic syndrome: A link from oxidative stress and inflammation to neurodegeneration. Synapse. 2017; doi: 10.1002/syn.21990

5. Andres RC, Helena BC, Juliana PP, et al. Diabetes-related neurological implications and pharmacogenomics. Current pharmaceutical design. 2017; doi: 10.2174/1381612823666170317165350
6. De La Monte SM. Metabolic derangements mediate cognitive impairment and Alzheimer's disease: role of peripheral insulin-resistance diseases. Panminerva medica. 2012; 54(3):171–8. doi. [PubMed: 22801434]
7. Lu M, Hu G. Targeting metabolic inflammation in Parkinson's disease: implications for prospective therapeutic strategies. Clinical and experimental pharmacology & physiology. 2012; 39(6):577–85. DOI: 10.1111/j.1440-1681.2011.05650.x [PubMed: 22126374]
8. Adams RH, Eichmann A. Axon guidance molecules in vascular patterning. Cold Spring Harbor perspectives in biology. 2010; 2(5):a001875.doi: 10.1101/cshperspect.a001875 [PubMed: 20452960]
9. Bartness TJ, Song CK. Thematic review series: adipocyte biology. Sympathetic and sensory innervation of white adipose tissue. Journal of lipid research. 2007; 48(8):1655–72. DOI: 10.1194/jlr.R700006-JLR200 [PubMed: 17460327]
10. Ryu V, Bartness TJ. Short and long sympathetic-sensory feedback loops in white fat. American journal of physiology Regulatory, integrative and comparative physiology. 2014; 306(12):R886–900. DOI: 10.1152/ajpregu.00060.2014
11. Bartness TJ, Ryu V. Neural control of white, beige and brown adipocytes. International journal of obesity supplements. 2015; 5(Suppl 1):S35–9. DOI: 10.1038/ijosup.2015.9 [PubMed: 27152173]
12. Rosen ED, Spiegelman BM. What we talk about when we talk about fat. Cell. 2014; 156(1–2):20–44. DOI: 10.1016/j.cell.2013.12.012 [PubMed: 24439368]
13. Giger RJ, Hollis ER 2nd, Tuszynski MH. Guidance molecules in axon regeneration. Cold Spring Harbor perspectives in biology. 2010; 2(7):a001867.doi: 10.1101/cshperspect.a001867 [PubMed: 20519341]
14. Ma CH, Omura T, Cobos EJ, et al. Accelerating axonal growth promotes motor recovery after peripheral nerve injury in mice. The Journal of clinical investigation. 2011; 121(11):4332–47. DOI: 10.1172/JCI58675 [PubMed: 21965333]
15. Scheib J, Hoke A. Advances in peripheral nerve regeneration. Nature reviews Neurology. 2013; 9(12):668–76. DOI: 10.1038/nrneurol.2013.227 [PubMed: 24217518]
16. Gaudet AD, Popovich PG, Ramer MS. Wallerian degeneration: gaining perspective on inflammatory events after peripheral nerve injury. Journal of neuroinflammation. 2011; 8:110.doi: 10.1186/1742-2094-8-110 [PubMed: 21878126]
17. Santos D, Giudetti G, Micera S, et al. Focal release of neurotrophic factors by biodegradable microspheres enhance motor and sensory axonal regeneration in vitro and in vivo. Brain research. 2016; 1636:93–106. DOI: 10.1016/j.brainres.2016.01.051 [PubMed: 26854135]
18. Eyjolfsdottir H, Eriksdotter M, Linderoth B, et al. Targeted delivery of nerve growth factor to the cholinergic basal forebrain of Alzheimer's disease patients: application of a second-generation encapsulated cell biodelivery device. Alzheimer's research & therapy. 2016; 8(1):30.doi: 10.1186/s13195-016-0195-9
19. Sorrell JM. Development of arteries in embryonic chick bone marrow with special reference to the appearance of periarterial granulopoietic sheaths. The Anatomical record. 1988; 221(3):730–6. DOI: 10.1002/ar.1092210308 [PubMed: 3189868]
20. Reichert B, Yasmeen R, Jeyakumar SM, et al. Concerted action of aldehyde dehydrogenases influences depot-specific fat formation. Mol Endocrinol. 2011; 25(5):799–809. me.2010-0465 [pii]. DOI: 10.1210/me.2010-0465 [PubMed: 21436255]
21. Yasmeen R, Jeyakumar SM, Reichert B, et al. The contribution of vitamin A to autocrine regulation of fat depots. Biochimica et biophysica acta. 2012; 1821(1):190–7. DOI: 10.1016/j.bbalip.2011.06.004 [PubMed: 21704731]
22. Yu S, Levi L, Siegel R, et al. Retinoic acid induces neurogenesis by activating both retinoic acid receptors (RARs) and peroxisome proliferator-activated receptor beta/delta (PPARbeta/delta). The Journal of biological chemistry. 2012; 287(50):42195–205. DOI: 10.1074/jbc.M112.410381 [PubMed: 23105114]

23. Bonet ML, Ribot J, Palou A. Lipid metabolism in mammalian tissues and its control by retinoic acid. Biochimica et biophysica acta. 2012; 1821(1):177–89. DOI: 10.1016/j.bbalip.2011.06.001 [PubMed: 21669299]
24. Yasmeen R, Reichert B, Deiuliis J, et al. Autocrine Function of Aldehyde Dehydrogenase 1 as a Determinant of Diet- and Sex-Specific Differences in Visceral Adiposity. Diabetes. 2012; doi: 10.2337/db11-1779
25. Kiefer FW, Vernochet C, O'Brien P, et al. Retinaldehyde dehydrogenase 1 regulates a thermogenic program in white adipose tissue. Nature medicine. 2012; 18(6):918–25. DOI: 10.1038/nm.2757
26. Fan X, Molotkov A, Manabe S, et al. Targeted disruption of Aldh1a1 (Raldh1) provides evidence for a complex mechanism of retinoic acid synthesis in the developing retina. Molecular and cellular biology. 2003; 23(13):4637–48. doi. [PubMed: 12808103]
27. Ziouzenkova O, Orasanu G, Sharlach M, et al. Retinaldehyde represses adipogenesis and diet-induced obesity. Nature medicine. 2007; 13(6):695–702. nm1587 [pii]. DOI: 10.1038/nm1587
28. Yang F, Zhang X, Maiseyeu A, et al. The prolonged survival of fibroblasts with forced lipid catabolism in visceral fat following encapsulation in alginate-poly-L-lysine. Biomaterials. 2012; 33(22):5638–49. DOI: 10.1016/j.biomaterials.2012.04.035 [PubMed: 22575837]
29. Gushchna L, Yasmeen R, Ziouzenkova O. Moderate vitamin A supplementation in obese mice regulates tissue factor and cytokine production in a sex-specific manner. Archives of Biochemistry and Biophysics. 2013; 539:239–47. DOI: 10.1016/j.abb.2013.06.020 [PubMed: 23850584]
30. Yasmeen R, Reichert B, Deiuliis J, et al. Autocrine function of aldehyde dehydrogenase 1 as a determinant of diet- and sex-specific differences in visceral adiposity. Diabetes. 2013; 62(1):124–36. DOI: 10.2337/db11-1779 [PubMed: 22933113]
31. Xu L, Shen Q, Mao Z, et al. Encapsulation Thermogenic Preadipocytes for Transplantation into Adipose Tissue Depots. Journal of visualized experiments : JoVE. 2015; (100):e52806.doi: 10.3791/52806 [PubMed: 26066392]
32. Davies SJ, Goucher DR, Doller C, et al. Robust regeneration of adult sensory axons in degenerating white matter of the adult rat spinal cord. The Journal of neuroscience : the official journal of the Society for Neuroscience. 1999; 19(14):5810–22. doi. [PubMed: 10407022]
33. Gensel JC, Nakamura S, Guan Z, et al. Macrophages promote axon regeneration with concurrent neurotoxicity. The Journal of neuroscience : the official journal of the Society for Neuroscience. 2009; 29(12):3956–68. DOI: 10.1523/jneurosci.3992-08.2009 [PubMed: 19321792]
34. Lerch JK, Martinez-Ondaro YR, Bixby JL, et al. cJun promotes CNS axon growth. Molecular and cellular neurosciences. 2014; 59:97–105. DOI: 10.1016/j.mcn.2014.02.002 [PubMed: 24521823]
35. Shen Q, Riedl KM, Cole RM, et al. Egg yolks inhibit activation of NF-kappaB and expression of its target genes in adipocytes after partial delipidation. Journal of agricultural and food chemistry. 2015; doi: 10.1021/jf5056584
36. Hernandez-Pedro N, Granados-Soto V, Ordonez G, et al. Vitamin A increases nerve growth factor and retinoic acid receptor beta and improves diabetic neuropathy in rats. Translational research : the journal of laboratory and clinical medicine. 2014; 164(3):196–201. DOI: 10.1016/j.trsl.2014.04.002 [PubMed: 24768685]
37. Peeraully MR, Jenkins JR, Trayhurn P. NGF gene expression and secretion in white adipose tissue: regulation in 3T3-L1 adipocytes by hormones and inflammatory cytokines. American journal of physiology Endocrinology and metabolism. 2004; 287(2):E331–9. DOI: 10.1152/ajpendo.00076.2004 [PubMed: 15100092]
38. Bullo M, Peeraully MR, Trayhurn P, et al. Circulating nerve growth factor levels in relation to obesity and the metabolic syndrome in women. Eur J Endocrinol. 2007; 157(3):303–10. DOI: 10.1530/EJE-06-0716 [PubMed: 17766712]
39. Molotkov A, Duester G. Genetic evidence that retinaldehyde dehydrogenase Raldh1 (Aldh1a1) functions downstream of alcohol dehydrogenase Adh1 in metabolism of retinol to retinoic acid. The Journal of biological chemistry. 2003; 278(38):36085–90. DOI: 10.1074/jbc.M303709200 [PubMed: 12851412]
40. Overman JJ, Clarkson AN, Wanner IB, et al. A role for ephrin-A5 in axonal sprouting, recovery, and activity-dependent plasticity after stroke. Proc Natl Acad Sci U S A. 2012; 109(33):E2230–9. DOI: 10.1073/pnas.1204386109 [PubMed: 22837401]

41. Hernandez-Miranda LR, Cariboni A, Faux C, et al. Robo1 regulates semaphorin signaling to guide the migration of cortical interneurons through the ventral forebrain. The Journal of neuroscience : the official journal of the Society for Neuroscience. 2011; 31(16):6174–87. DOI: 10.1523/JNEUROSCI.5464-10.2011 [PubMed: 21508241]
42. Janes PW, Saha N, Barton WA, et al. Adam meets Eph: an ADAM substrate recognition module acts as a molecular switch for ephrin cleavage in trans. Cell. 2005; 123(2):291–304. DOI: 10.1016/j.cell.2005.08.014 [PubMed: 16239146]
43. Hattori M, Osterfield M, Flanagan JG. Regulated cleavage of a contact-mediated axon repellent. Science. 2000; 289(5483):1360–5. doi. [PubMed: 10958785]
44. Chang TM. Pharmaceutical and therapeutic applications of artificial cells including microencapsulation. Eur J Pharm Biopharm. 1998; 45(1):3–8. S0939-6411(97)00117-3 [pii]. DOI: 10.1016/S0939-6411(97)00117-3 [PubMed: 9689530]
45. Chang TMS. Semipermeable microcapsules. Science. 1964; 146:524–5. doi. [PubMed: 14190240]
46. Cortez M, Singleton JR, Smith AG. Glucose intolerance, metabolic syndrome, and neuropathy. Handbook of clinical neurology. 2014; 126:109–22. DOI: 10.1016/B978-0-444-53480-4.00009-6 [PubMed: 25410218]
47. Giordano A, Cesari P, Capparuccia L, et al. Sema3A and neuropilin-1 expression and distribution in rat white adipose tissue. J Neurocytol. 2003; 32(4):345–52. DOI: 10.1023/B:NEUR.0000011328.61376.bb [PubMed: 14724377]
48. Kang SK, Shin MJ, Jung JS, et al. Autologous adipose tissue-derived stromal cells for treatment of spinal cord injury. Stem Cells Dev. 2006; 15(4):583–94. DOI: 10.1089/scd.2006.15.583 [PubMed: 16978061]
49. Kir S, White JP, Kleiner S, et al. Tumour-derived PTH-related protein triggers adipose tissue browning and cancer cachexia. Nature. 2014; 513(7516):100–4. DOI: 10.1038/nature13528 [PubMed: 25043053]
50. Randall JC, Winkler TW, Kutalik Z, et al. Sex-stratified genome-wide association studies including 270,000 individuals show sexual dimorphism in genetic loci for anthropometric traits. PLoS genetics. 2013; 9(6):e1003500.doi: 10.1371/journal.pgen.1003500 [PubMed: 23754948]
51. Zeggini E, Scott LJ, Saxena R, et al. Meta-analysis of genome-wide association data and large-scale replication identifies additional susceptibility loci for type 2 diabetes. Nat Genet. 2008; 40(5):638–45. DOI: 10.1038/ng.120 [PubMed: 18372903]
52. Zhao J, Bradfield JP, Zhang H, et al. Examination of all type 2 diabetes GWAS loci reveals HHEX-IDE as a locus influencing pediatric BMI. Diabetes. 2010; 59(3):751–5. DOI: 10.2337/db09-0972 [PubMed: 19933996]

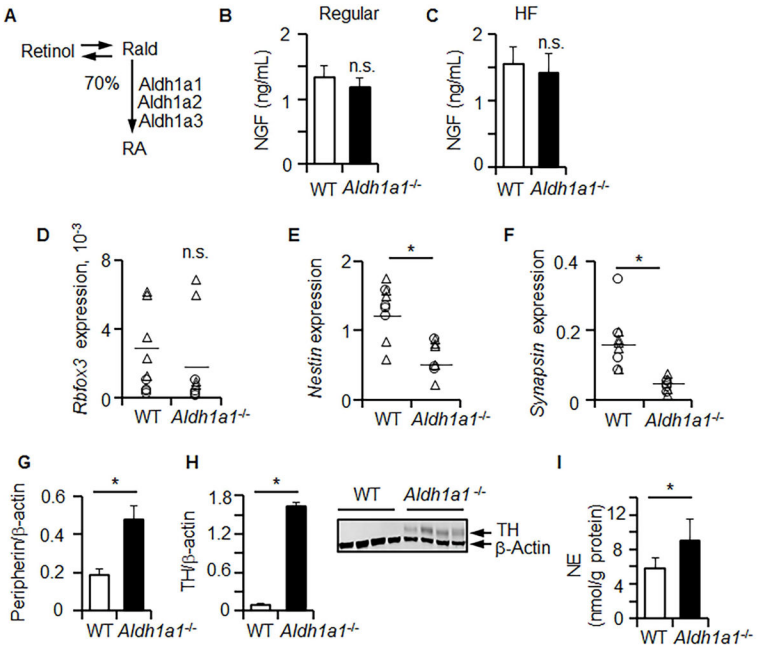

Figure 1. *Aldh1a1* deficiency induces innervation in WAT in vivo without an increase in neural precursors

(A) Schematic of the main processes leading to production of retinoic acid (RA) in WAT. ALDH1A1 produces 70% of RA which activates RAR in adipocytes (100%) [20]. NGF plasma levels were examined by ELISA in WT and *Aldh1a1*$^{-/-}$ mice fed regular chow (B) or HF diet (C), n=4 per group randomly selected from Study 1 and 2. Relative expressions of *Rbfox3* (D), *Nestin* (E), and *Synopsin* (F) were measured in iAb WAT from WT and *Aldh1a1*$^{-/-}$ males (triangle, n=5) and females (circle, n=5) by TaqMan RT-PCR (HF, Study 1). Expressions were normalized to Tata box protein (TBP). The levels of peripherin (G) and tyrosine hydroxylase (TH) (H) were analyzed by Western blot from randomly selected tissues of WT (n=4) and *Aldh1a1*$^{-/-}$ mice (n=4) (HF, Study 1). Protein expression was normalized by levels of housekeeping genes (β-actin). The insert shows representative Western blot. (I) Norepinephrine (NE) level from iAb fat pat homogenates in WT (n=6) and *Aldh1a1*$^{-/-}$ mice (n=5) was measured using ELISA (HF diet, Study 1). An asterisk indicates a significant difference between WT and *Aldh1a1*$^{-/-}$ groups (p<0.05). n.s.: not significant, Mann-Whitney U test.

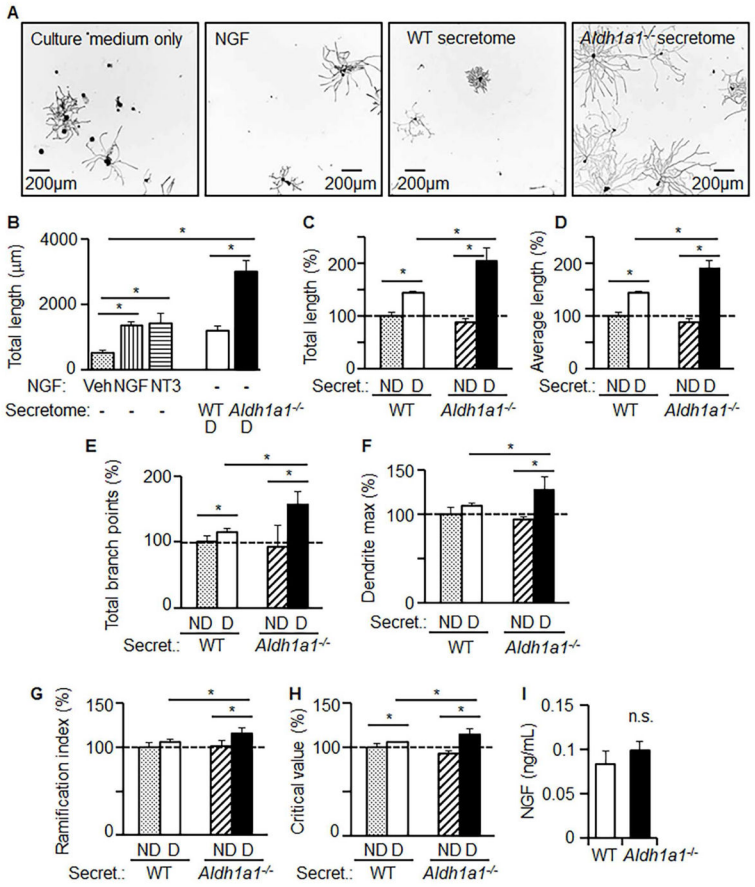

Figure 2. Secretome of *Aldh1a1*$^{-/-}$ thermocytes promotes axon growth in DRG neurons in vitro

DRG neurons (500 neurons per well) were cultured in DRG culture medium only, or DRG culture medium with NGF (10ng/mL), or DRG culture medium with WT secretome (1/1, v/v), or DRG culture medium with *Aldh1a1*$^{-/-}$ secretome (1/1, v/v) for 24 hours. WT and *Aldh1a1*$^{-/-}$ adipocytes were differentiated for 5 days. The secretome is the media collected from these fully-differentiated cells after 24h of incubation. Neurite outgrowth parameters were assayed using a Thermo Scientific™ ArrayScan™ XTI Live High Content microscope and analyzed with the Neuronal Profiling Algorithm. Nine independent experiments were performed using DRG from three mice. Each DRG batch was analyzed in triplicate. Asterisks indicate P<0.05 between different groups; Mann-Whitney U test. Representative images (A) and quantification of neurite length (B) were taken in neurons 24 hours after stimulation. (C–F) Axon guidance effects of secretomes from non-differentiated WT (ND, dotted bars) and *Aldh1a1*$^{-/-}$ (ND, upward hatched bars) preadipocytes, and differentiated (D, 5 days) WT (white bars) and *Aldh1a1*$^{-/-}$ (black bars) adipocytes on DRG neurons. Total length (C), average length (D), total branch points (E), dendrite maximum length (F), ramification index (G), as well as critical value (H) were measured in DRG neurons and analyzed by Neuronal Profiling Algorithm. (I) NGF levels in media collected from differentiated WT and *Aldh1a1*$^{-/-}$ adipocytes (n=4 per group) were analyzed by ELISA. Data show mean ± SD obtained with one DRG batch. Asterisks indicate P<0.05 between different groups; Mann-Whitney U test.

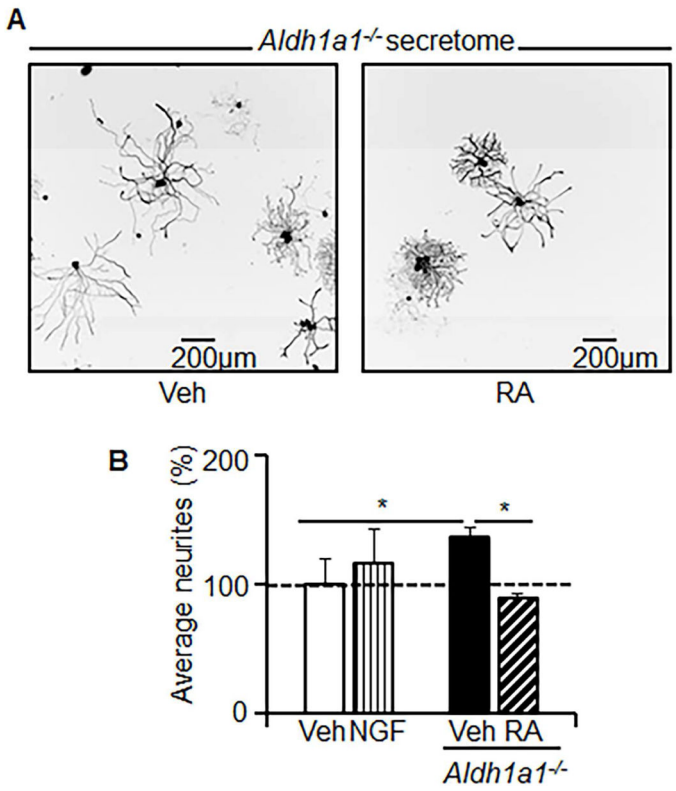

Figure 3. The axon-growth supportive milieu of *Aldh1a1*$^{-/-}$ secretome is RA-dependent

DRG neurons were cultured in DRG culture medium with the secretome from *Aldh1a1*$^{-/-}$ adipocytes (1/1, v/v) that were treated with or without RA (100nM). RA was added to *Aldh1a1*$^{-/-}$ differentiation medium (Day 0, 2, 5). To prepare this secretome, medium was collected for the last 24 hours. (A) Representative images were selected from 3 independent experiments. (B) Mean neurite growth indices were measured by XTI microscopy in DRG neurons in DRG culture medium containing Veh (vehicle, white bar), NGF (vertical lined bar), or *Aldh1a1*$^{-/-}$ secretome treated without (black bar) or with RA (hatched bar). An asterisk indicates $P<0.05$; Mann-Whitney U test.

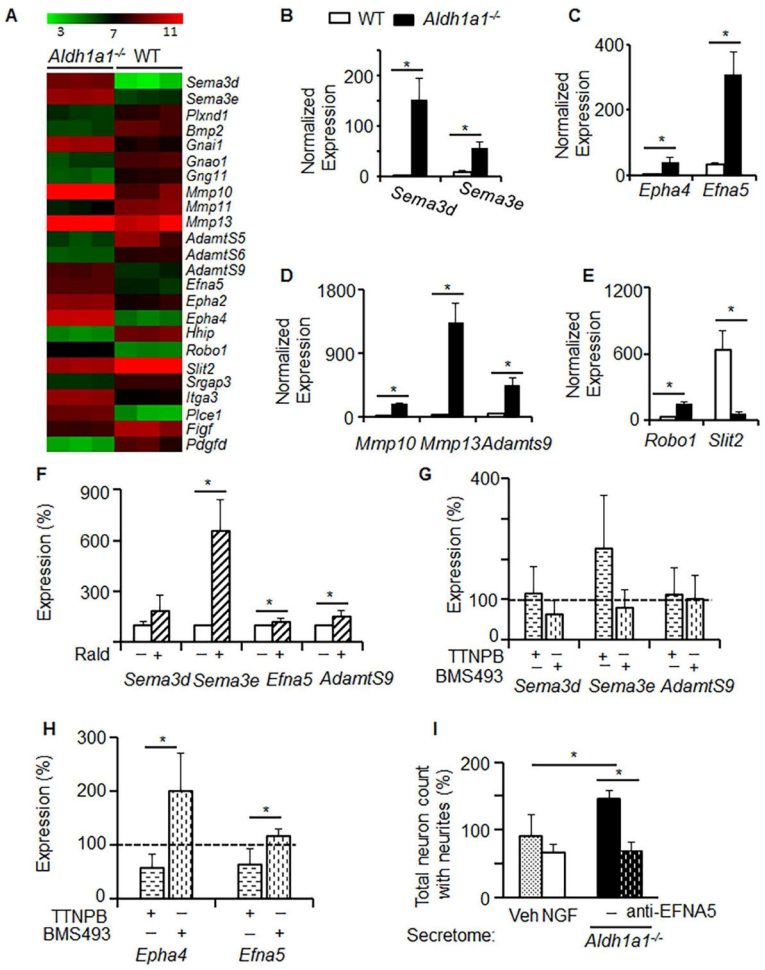

Figure 4. *Aldh1a1*$^{-/-}$ adipocytes express axon guidance molecules regulated by RAR

(A) Expression heat map reveals differences in expression of axon guidance cluster of genes between WT and *Aldh1a1*$^{-/-}$ preadipocytes (n=3 per group). Transcript analysis was performed by Affymetrix microarray. The axon guidance cluster was identified by Ingenuity Pathway Analysis. (B–E) WT (white bars) and *Aldh1a1*$^{-/-}$ (black bars) preadipocytes (n=3) were differentiated for 4 days. Expressions of *Sema3d* and *Sema3e* (B); *Epha4* and *Efna5* (C); *Mmp10, Mmp13,* and *Adamts9* (D); *Robo1* and *Slit2* (E) were measured in purified mRNA samples using a customized NanoString mouse panel including markers for adipogenesis, thermogenesis, and axon guidance genes. Data represent mean±SD. An asterisk indicates p<0.05; Mann Whitney U test. (F–H) 3T3-L1 adipocytes were cultured in differentiation medium for 4 days. At day 5, medium was replaced by UV-treated 1% FBS-containing DMEM with and without Rald (30nM) (F), or with and without TTNPB (50nM) or BMS493 (100nM) (G–H). 24 hrs post stimulation, cells were harvested for mRNA. Gene expression was measured by the NanoString mouse innervation panel. Data (mean±SD, n=3) were normalized to the levels found in non-treated control (100%, dashed line). An asterisk indicates p<0.05; Mann-Whitney U test. (I) Neuron growth indexes were obtained by XTI microscopy in DRG neurons cultured in DRG culture medium with or without NGF or in the

Aldh1a1$^{-/-}$ secretome (1/1, v/v) with and without blocking antibody against EFNA5 (1μg/mL) for 24 hours.

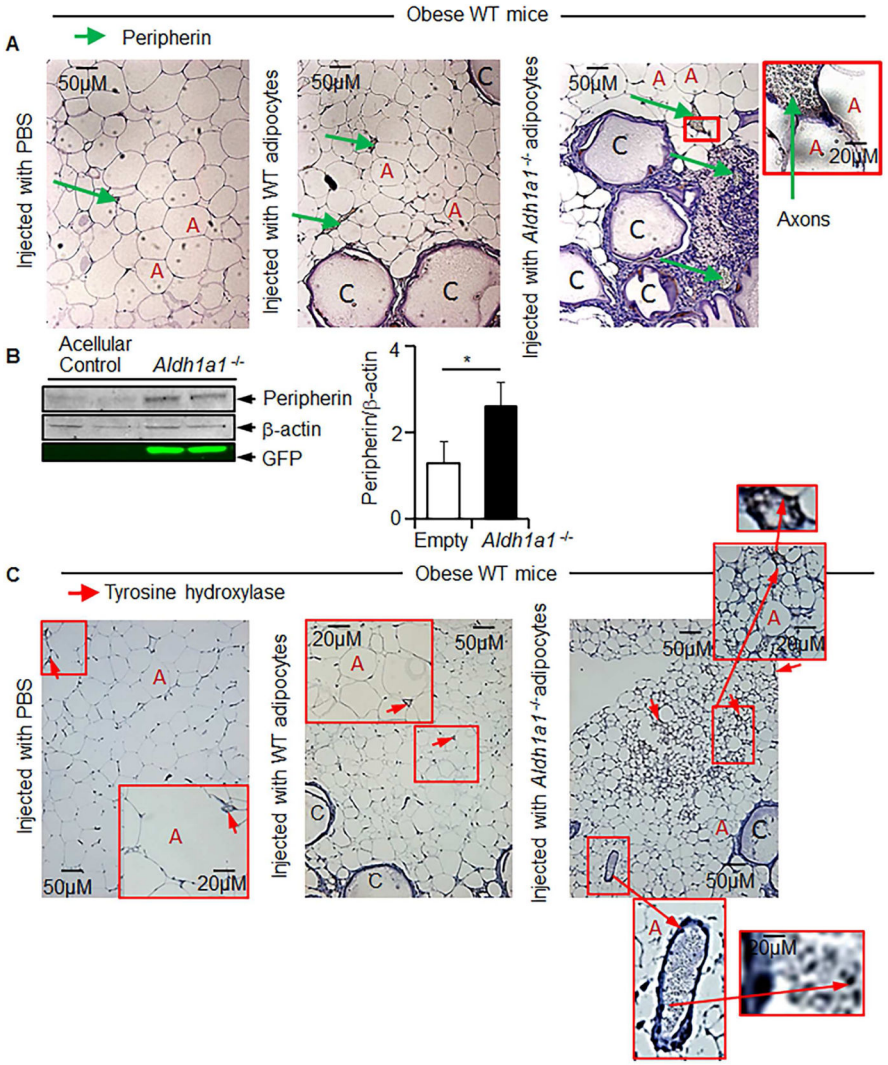

Figure 5. Secretome of grafted encapsulated *Aldh1a1*$^{-/-}$ adipocytes promotes innervation in WAT in WT obese mice

Obese WT female mice (n=18) on a HF diet were treated with acellular (n=3) microcapsules or micro capsules containing WT (n=5) or *Aldh1a1*$^{-/-}$ adipocytes (n=5) or mice remained untreated (n=5) (Study 3). (A) Immunohistochemical analysis of peripherin protein levels in axons in iAb WAT of the animal groups in Study 3. (A) Representative images of peripherin (brown) immunoreactive areas of nerves in paraffin-embedded iAb fat from mice injected with vehicle and encapsulated WT and *Aldh1a1*$^{-/-}$ cells at 20× magnification. Green arrows indicate examples of peripherin-positive axons of nerves at 40× magnification. 'C' indicates empty core of microcapsules because encapsulated cells are attached at the inner surface of capsules. The 'A' letters show examples of adipocytes. (B) Peripherin was analyzed by Western blot in whole homogenized iAb WAT pads from mice in Study 3. Bars show peripherin levels from the same tissues normalized to β-actin levels (n=4). An asterisk indicates a significant difference between empty and *Aldh1a1*$^{-/-}$ groups (p<0.05; Mann-Whitney U test). (C) Immunohistochemical analysis of tyrosine hydroxylase (TH, brown) protein levels in axons of the animal groups in Study 3. Note that TH-positive areas are

found within nerves (40×) (red arrow) or in areas containing numerous multilocular adipocytes.

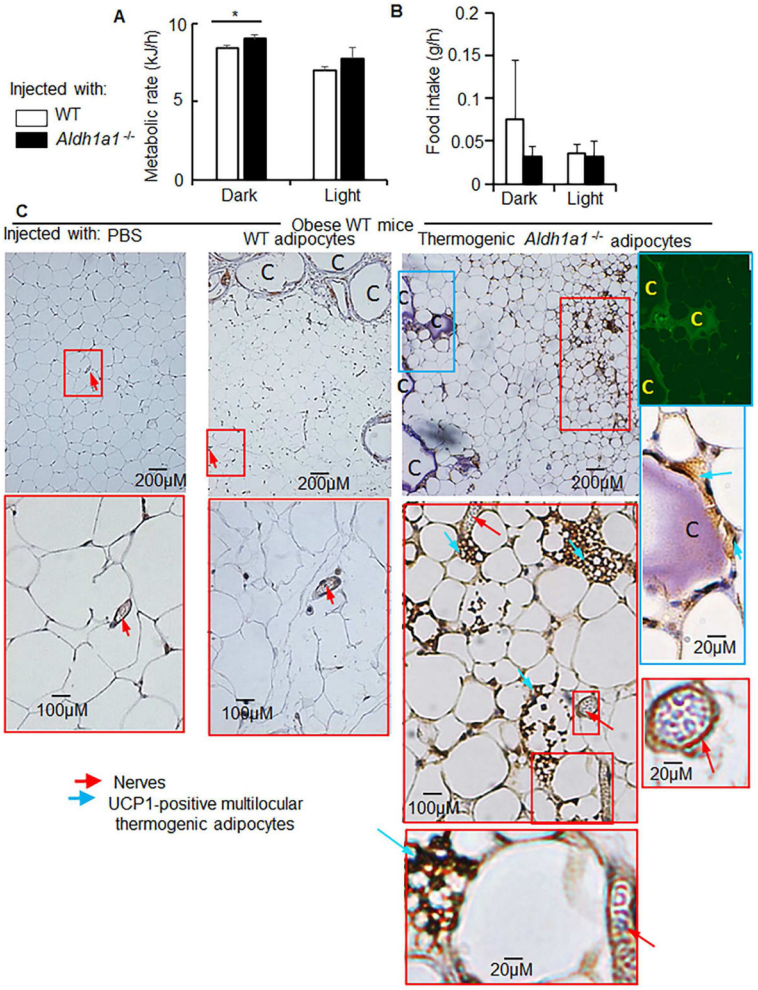

Figure 6. Secretome of grafted encapsulated *Aldh1a1*$^{-/-}$ adipocytes regulated metabolism and thermogenic properties of WAT in WT obese mice

Metabolic rate (A) and food intake (B) in the same obese WT mice treated with encapsulated WT adipocytes (white bar) or *Aldh1a1*$^{-/-}$ adipocytes. Asterisk indicates statistically significant differences in metabolic rate during the dark period between treated groups (Wilcoxon-Mann-Whitney Rank test, $p<0.05$, $n=4$). Food intake was not significantly different between groups.

(C) Immunohistochemical analysis of UCP1 levels (marker of thermogenesis) in paraffin-embedded iAb fat from mice injected with vehicle, encapsulated WT, and encapsulated *Aldh1a1*$^{-/-}$ cells at 20× magnification. Inserted figure shows the example of UCP-1 positive multilicular adipocytes at 40× magnification. These UCP-1 positive thermogenic multilicular adipocyte areas (blue arrows) were localized in proximity of nerves (red arrows). Right insert: *Aldh1a1*$^{-/-}$ adipocytes inside capsules (indicated by C) also expressed UCP-1.